Broadband acoustic attenuation in microperforated metashells with ventilation $\ensuremath{ igoplus }$

Special Collection: Fundamentals and Applications of Metamaterials: Breaking the Limits

Jiaji Chen; Yonghui Zhang; Yukai Yu; ... et. al



Appl. Phys. Lett. 122, 231701 (2023) https://doi.org/10.1063/5.0152725





CrossMark

Integrates all
Instrumentation + Software
for Control and Readout of

Superconducting Qubits

NV-Centers

Spin Qubits

Spin Qubits

Spin Qubits Setup



Broadband acoustic attenuation in microperforated meta-shells with ventilation

Cite as: Appl. Phys. Lett. **122**, 231701 (2023); doi: 10.1063/5.0152725 Submitted: 31 March 2023 · Accepted: 23 May 2023 · Published Online: 5 June 2023







Jiaji Chen, DYOnghui Zhang, Yukai Yu, DYao Zhai, Huy Nguyen, DSharon Tracy, DShar

AFFILIATIONS

- Department of Mechanical and Aerospace Engineering, University of Missouri, Columbia, Missouri 65211, USA
- ²Key Laboratory of Dynamics and Control of Flight Vehicle of Ministry of Education, School of Aerospace Engineering, Beijing Institute of Technology, Beijing 100081, China

Note: This paper is part of the APL Special Collection on Fundamentals and Applications of Metamaterials: Breaking the Limits.

^{a)}Authors to whom correspondence should be addressed: huangg@missouri.edu and zhxming@bit.edu.cn

ABSTRACT

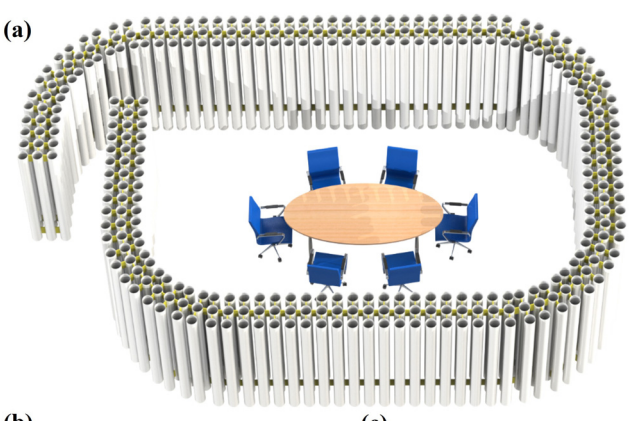
Achieving sound attenuation across a broad frequency range while maintaining adequate ventilation remains a significant challenge in acoustic engineering, as there exists a rigid trade-off between attenuation ability and ventilation. In this Letter, we propose a double-layered microperforated meta-shells to serve as broadband acoustic ventilation barrier. Multiple scattering theory is first employed to characterize sound attenuation performance of the proposed design in terms of both sound absorption and transmission loss, which is not reported before. Experimental result demonstrates a good enhancement of absorption due to the insertion of inner shell with a specific perforation rate of micro cores. The mechanism can be attributed to the inter-cell coupling, which is further utilized to devise a different configuration by wrapping the meta-shell with porous sponge. It is found that adding an extra layer of sponge can further improve the low-frequency attenuation performance. The proposed broadband sound barrier with effective ventilation can find potential applications in architectural acoustics and office noise insulation.

Published under an exclusive license by AIP Publishing. https://doi.org/10.1063/5.0152725

Conventional airborne sound attenuation essential in acoustic barriers refers to either reflecting or absorbing the incident acoustic energy while blocking airflow transport. The modern needs require sound attenuation while preserving high-efficiency ventilation, such as office acoustics, where acoustic barrier that blocks unwanted noises without compromising the indoor air quality is required. However, most of the conventional sound barriers failed to ventilate as they block both sound and air flow at the same time. 1-3 Thus, there has been a shift in research focus toward acoustic ventilation barriers over the past few years. In pursuit of acoustic ventilation barriers, a common approach is to design a window allowing airflow to pass with sound absorbing components (Helmholtz resonator, space-coiling, etc.) on the wall of the window. Similar acoustic ventilation barriers based on Helmholtz resonators,4 membranes, 8,9 and Fano-like interference 10-12 have been proposed. However, most existing acoustic ventilation barriers only work in narrow frequency bands. Despite efforts to broaden the working frequency range, resulting designs have either exhibited a limited bandwidth ¹³ or a poor airflow passage. ¹⁴ Design of broadband acoustic ventilation barriers remains challenging in the noise control area.

Sonic crystals belong to an alternative configuration widely studied for achieving acoustic attenuation, and have been used as traffic noise barriers. They consist of periodically arranged rigid rods such that, due to the Bragg scattering, sonic crystals induce bandgaps, and noises within gap frequencies are prohibited to propagate. Sonic crystals have natural advantages in terms of optical transparency and airflow permeability. They also have good adaptation to changes in application environments as their performances are robust to weak non-periodic arrangement of scattering elements, as shown in Fig. 1(a). However, conventional sonic crystals are usually made with rigid rods, meaning that they are only effective in bandgap frequencies, and are bulky when controlling low-frequency noises. To overcome the challenges, Garcia introduced the idea of microperforated shells for acoustic attenuation. ¹⁶

³Materials Innovation, Steelcase Inc., Grand Rapids, Michigan 49508, USA



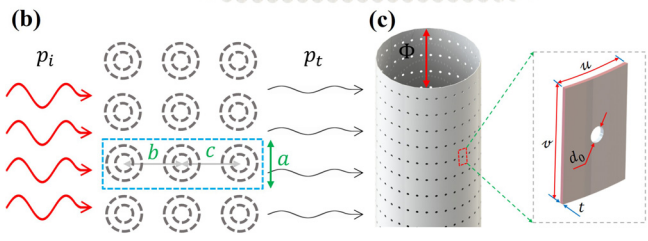


FIG. 1. (a) Schematic illustration of microperforated shells in open office application. (b) Top view of microperforated meta-shells array. The meta-shells undergo an acoustic incident wave from the left (red arrows) and the transmitted wave to the right (green arrows). The corresponding lattice constants are indicated. (c) Side view of a single microperforated cylinder meta-shell, with all the geometric parameters indicated in the inset. In this case, perforation rate $\sigma = \pi d_0^2/(4uv)$.

Flat microperforated panels (MPPs) were rolled into a cylindrical shell acting as the cell element of sonic crystals, on which arrays of submillimetric orifices along the panel absorb acoustic energy.

In this Letter, more in-depth studies are devoted to microperforated meta-shells for broadband acoustic attenuation including both wave absorption and transmission loss. We begin the study by extending the classical single MPP meta-shell model¹⁶ to double MPP metashell structure for further enhancing sound absorption and attenuation capability, as shown in Fig. 1(b). Cell element of sonic crystals consists of the outer and inner MPP shells. For simplicity, the radius of inner shell is set to half that of outer shell for fabrication convenience. Further acoustic attenuation potential for selecting the best inner shell dimension can be released through numerical optimizations. Theoretical model based on multiple scattering theory (MST) is developed for double MPP meta-shell structures. Multiple scattering model, which includes the coupling of all scattering channels, has been demonstrated to be efficient and accurate in evaluating sound performance of sonic crystals. 6 Meta-shells with cylindrical cores are considered in this study, and they can be well modeled by acoustic impedance with the formula first proposed by Maa.¹⁷ Thus, theoretical model developed here is free from the fitting procedure to determine microstructural parameters. 10

We briefly outline the multiple scattering model as follows. Based on Maa's theory for a microperforated panel surrounded by air with density ρ_0 and speed of sound c_0 , its acoustic impedance reads¹⁷

$$Z_p = (r + i\omega m)\rho_0 c_0, \tag{1}$$

where

$$r = \frac{32\eta t}{\sigma \rho_0 c_0 d_0^2} k_r, \quad k_r = \left(1 + \frac{K^2}{32}\right)^{\frac{1}{2}} + \frac{\sqrt{2} K d_0}{32 t}$$

$$\omega m = \frac{\omega t}{\sigma c_0} k_m, \quad k_m = \left(1 + \frac{K^2}{2}\right)^{-\frac{1}{2}} + 0.85 \frac{d_0}{t}$$
(2)

and

$$K = d_0 \sqrt{\frac{\omega \rho_0}{4\eta}},\tag{3}$$

where d_0 is the diameter of perforation, ω is the angular frequency of sound, η is the dynamic viscosity of air, t is the thickness of panel, and σ is the perforation rate. Equation (1) for acoustic impedance fundamentally links changes in sound pressure and normal velocity along the perpendicular axis of a microperforated panel. Consequently, the relationship between pressure and the normal velocity across the cylindrical shell is governed by the same equation.

As shown in Fig. 1(c), the microperforated shell has an outer diameter of Φ . The radius of shell is defined between outer radius R^+ and inner radius R^- , where $R^+ = \Phi/2$ and $R^- = R^+ - t$. The shell has impedance Z_p corresponding to Eq. (1). The acoustic pressure field inside/outside the shell (P_{in}/P_{out}) can be expressed as an infinite sum of Bessel function and Hankel function in cylindrical coordinate as

$$P_{in}(r,\phi) = \sum_{n=-\infty}^{+\infty} A_n J_n(kr) e^{in\phi}, \quad (r < R^-), \tag{4}$$

$$P_{out}(r,\phi) = \sum_{n=-\infty}^{+\infty} B_n J_n(kr) e^{in\phi} + \sum_{n=-\infty}^{+\infty} C_n H_n(kr) e^{in\phi}, \quad (r > R^+),$$
(5)

where $k = \omega/c_0$ is the wavenumber of sound in air, and J_n and H_m here, represent the nth order Bessel function of the first kind and Hankel function of the first kind, respectively. The boundary conditions through the microperforated shell are based on the continuity of normal velocity across the shell and the relation between pressure and velocity given by the acoustic impedance. This can be expressed as

$$v_{in}(R^{-}) = v_{out}(R^{+}) = \frac{P_{out}(R^{+}) - P_{in}(R^{-})}{Z_{p}}.$$
 (6)

Combining Eqs. (1), (4), (5), and (6), the T-matrix of microperforated cylindrical shell can be obtained as

$$T_n^{(1)} = \frac{C_n}{B_n} = -\frac{a_n J_n'(kR^+) - J_n(kR^+)}{a_n H_n'(kR^+) - H_n(kR^+)}$$
(7)

and

$$a_n = \frac{J_n(kR^-)}{J'_n(kR^-)} - \frac{iZ_p k}{\omega \rho_0}.$$
 (8)

We can use a similar method to find the T matrix for a scatterer, which consists of an outer shell and an inner shell. The results, T matrix reads

$$T_n^{(2)} = -\frac{b_n J_n'(kR_b^+) - J_n(kR_b^+)}{b_n H_n'(kR_b^+) - H_n(kR_b^+)} \tag{9}$$

and

$$b_n = \frac{J_n(kR_b^-) + T_n^{(1)}(R_a)H_n(kR_b^-)}{J'_n(kR_b^-) + T_n^{(1)}(R_a)H'_n(kR_b^-)} - \frac{iZ_pk}{\omega\rho_0}.$$
 (10)

Here, R_a and R_b stand for the radius of outer shell and inner shell, respectively. +/- sign represents outer/inner radius. $T_n^{(1)}(R_a)$ denotes the T matrix for inner shell. After T-matrix being determined, we can construct an interaction matrix that defines the coupling between each scatterer. More details can be found in Ref. 18.

As a calculation example, consider structural parameters b = c= 114 mm, a = 110 mm, $d_0 = 0.15$ mm, $\sigma = 0.05$, t = 1 mm, Φ = 76 mm, and u = v = 0.353 mm. Figure 2(a) shows theoretical results of sound absorption and transmission loss spectra for three layers of double-shell structures. Results show that the microperforated meta-shell array has high absorption and high sound transmission loss (STL) performances over extremely broad frequency band. Here, sound transmission loss (STL) is defined as STL = -20 $\times log_{10}|P_t/P_{in}|\text{,}$ and absorption coefficient is calculated by $\alpha=1$ $-|P_r/P_{in}|^2$, where P_{in} , P_t , P_r are the pressures for incident plane, transmitted, and reflected waves, respectively. Notice that these calculated results have involved the effect of different orders of scattering modes. A rectangular waveguide with the width equal to the periodicity a is employed to simulate acoustic performances. To evaluate the influence of the incident plane wave, numerical simulations are conducted for the waveguide system installed with a double-shell super cell, as illustrated in the inset of Fig. 2(a). It is worth mentioning that we use the effective impedance model [Eq. (1)] to simulate the metashells. Since diameter of the perforations and the overall shell size are under different length scale, numerical simulation built on a real

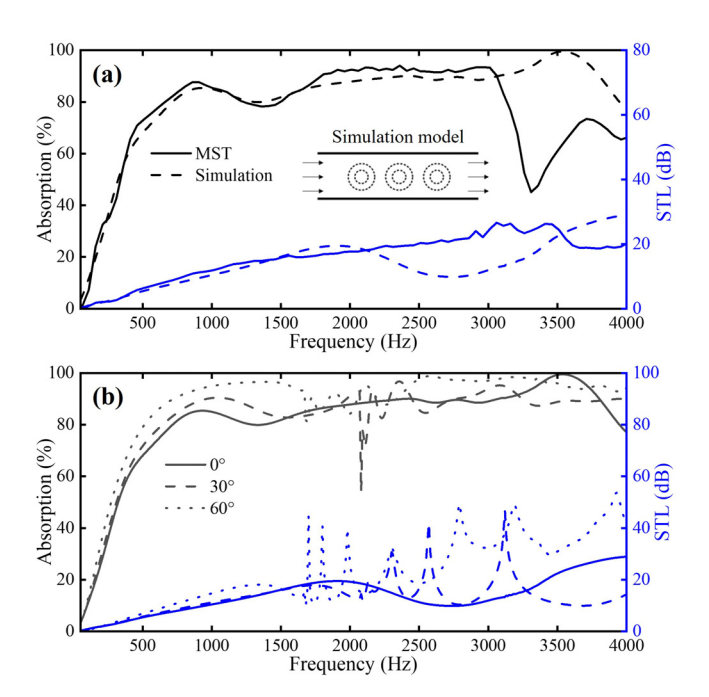


FIG. 2. (a) Sound absorption and transmission loss spectra calculated from multiple scattering theory and numerical simulation for three layers of double MPP metashell structures. (b) Numerical results of sound absorption and transmission loss spectra for plane wave incident at different angles.

microperforated meta-shell could demand substantial computational resources. The simulated result has been provided in Fig. 2(a), and it shows good agreement with the theoretical result in low-frequency region (up to 2000 Hz). This concludes the fact that acoustic performance of sonic crystals made of double-shell units can be characterized by that of a super cell in the waveguide system in certain frequency range below a cutoff and thus allows us to perform experimental studies in the waveguide system. In the meantime, the acoustic performance of the system for oblique incidence is numerically evaluated as shown in Fig. 2(b). The figure clearly demonstrates that the overall acoustic performance of the system for oblique incidence is nearly identical to that for normal incidence across most of the considered frequencies. However, we do observe improved sound insulation performance at certain frequencies when compared to the results for normal incidence. This improvement could be attributed to the enhanced multiple wave scattering along the oblique wave paths.

Figure 3(a) shows the impedance tube of rectangular cross section used to measure acoustic performance using the four-transducer method. The waveguide has the width a = 110 mm, which is the same as the lattice constant of sonic crystals, and the height h = 40 mm. The wave vector k_z along the waveguide direction is given by $k_z = \sqrt{(\omega/c_0)^2 - (k_{xl}^2 + k_{ym}^2)}$, where $k_{xl} = l\pi/a$, $k_{ym} = m\pi/h$, and l and m are natural numbers. For the lowest-order propagating mode, the cutoff frequency is found by setting l=1 and m=0, leading to $f_{cutoff} = (c_0/2)\sqrt{(l/a)^2 + (m/h)^2} = 1560$ Hz. To facilitate sample installation, a skylight is opened in the middle of the waveguide, which can accommodate one, two, or three cells with intercellular spacing b and c. The waveguide is sealed with a cover plate after the sample is installed. The meta-shells are fabricated by punching cylindrical cores on stainless steel round pipes with a high-precision laser drilling machine. The magnified partial view of MPP shells is shown in the inset of Fig. 3(a), where the horizontal and vertical spacings, i.e., u and ν , between adjacent holes, and the core diameter d_0 , are measured using a digital microscope. The sample photographs are shown in Figs. 3(b)-3(d).

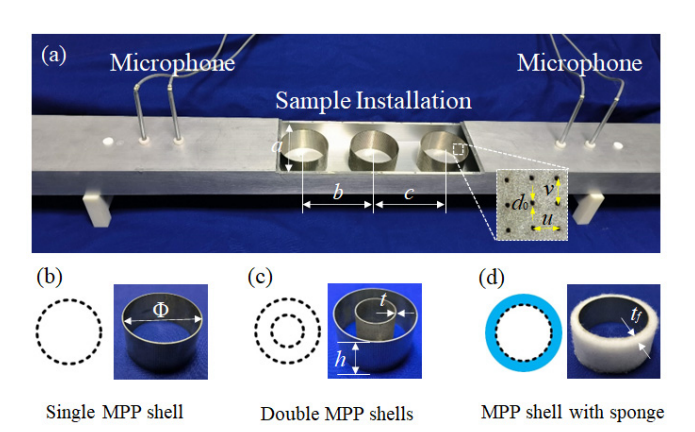


FIG. 3. (a) Acoustic impedance waveguide of rectangular cross section developed for measurement of MPP-shell structures. Schematic and sample photo of three different configurations: (b) single MPP meta-shell, (c) double MPP meta-shell, and (d) single MPP meta-shell wrapped with porous sponge.

Notice that the waveguide is only suitable for evaluating sound insulation performance under plane wave incidence. The wave scattered by an infinite array of supercells is equivalent to that of a supercell in waveguide under periodic boundary condition, whereas the experimental waveguide has a hard boundary condition. Due to the geometric symmetry in the meta-shells and waveguide, under normal plane wave incidence, scattered waves in the periodic waveguide are identical to those in the hard boundary waveguide. However, absorption and transmission loss for the oblique incidence can only be evaluated with a free-field measurement of the sample with many supercells but not with the current waveguide system. This issue would be the interest of our future study.

We first evaluate acoustic performance of single MPP shell with $\Phi = 76$ mm, b = c = 114 mm, $d_0 = 0.17$ mm, u = 1 mm, and v = 1 mm. Figure 4(a) shows both simulated and measured results of sound absorption and STL spectra for samples comprising one, two, or three unit cells. Measured results show good agreements with simulated ones except for some small deviations due to manufacturing defects. As the cell number increases, the bandwidth for sound

absorption has been obviously expanded with a significant enhancement at around 800 Hz. This can be explained by coupling between acoustic cavities within the shell and multiple scattering between shell scatterers. As cell number increases, acoustic waves bounce among scatterers to dissipate more energy via the thermal viscosity, thus explaining the broadband nature of our proposed design. Then, we insert an inner MPP shell with a diameter of 38 mm as an attempt to further enhance the absorption capability, and the measured results are shown in Fig. 4(b). However, the double layer meta-shell does not make great improvement in either absorption or STL compared with single layer sample. Therefore, we can conclude that the outer shell plays a dominant role in the acoustic attenuation compared with the inner shell.

As a further investigation, the meta-shells with a different set of core spacing u=1.9 mm and v=1.85 mm are fabricated, which corresponds to a lower perforation rate. Acoustic performance results are shown in Figs. 5(a) and 5(b) for single-shell and double-shell cases, respectively. Compared with Fig. 4(a), the overall absorption capability of single shell sample is degraded as can be attributed to lower

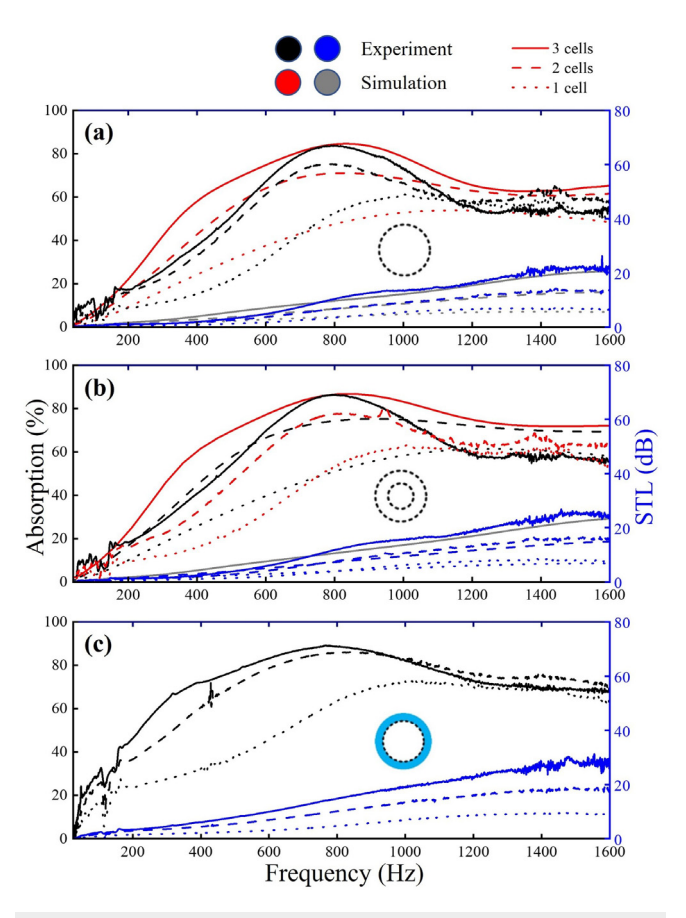


FIG. 4. (a)–(c) Measured frequency spectra of absorption coefficient and sound transmission loss (STL) for three different configurations corresponding to the model in Figs. 3(b)–3(d). Both experimental measurements (black and blue curves) and simulation results (red and gray curves) are shown in (a) and (b). Samples with different cell numbers have been measured for each configuration. The fabricated MPP meta-shells have the core spacing $u=1\,\mathrm{mm}$ and $v=1\,\mathrm{mm}$.

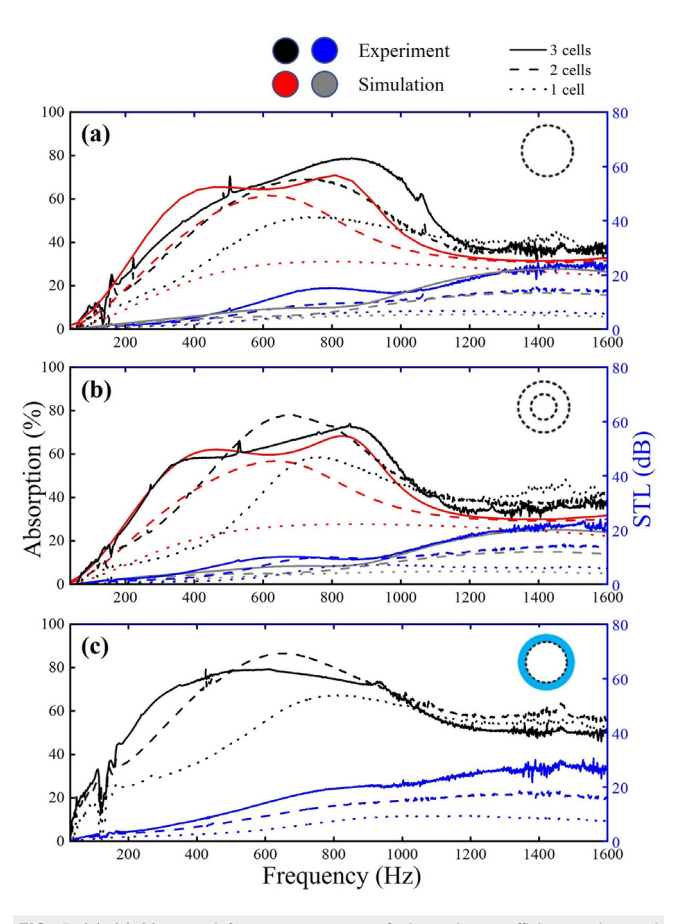


FIG. 5. (a)–(c) Measured frequency spectra of absorption coefficient and sound transmission loss (STL) for three different configurations corresponding to the model in Figs. 3(b)–3(d). Both experimental measurements (black and blue curves) and simulation results (red and gray curves) are shown in (a) and (b). Samples with different cell number have been measured for each configuration. The fabricated MPP meta-shells have the core spacing $u=1.9\,\mathrm{mm}$ and $v=1.85\,\mathrm{mm}$.

perforation rate of micro cores. However, addition of an inner shell causes a significant change in absorption spectrum for the sample with three unit cells, as seen in Fig. 5(b). For this case, a significant enhancement due to the insertion of inner shell is observed at low frequency near $400\,\mathrm{Hz}$. The signature is completely different from that of the sample concerned in Fig. 4(b), and can be attributed to the remarkable inter-cell coupling.

Inspired by the inter-cell coupling, we devise a different configuration by adding a layer of sponge to each meta-shell element, as shown in Fig. 3(d) for the model schematic and sample photo. A layer of porous sponge with a thickness of $t_f = 8.6$ mm is wrapped outside the MPP meta-shell of diameter 76 mm. Figures 4(c) and 5(c) show measured results of sound absorption and STL spectra for samples with different perforation rates. Compared to the model without sponge, adding extra layers of sponge can significantly improve the low-frequency absorption with broader bandwidth especially when more units are installed. This benefits from the damping enhancement assisted by the inter-cell coupling. It is noteworthy that the STL that exceeds 10 dB can be realized in a broad frequency range when at least two unit cells are used for all cases analyzed earlier. As for the ventilation efficiency, since we distribute meta-shells with a diameter of 76 mm in an array with lattice constant a = 110 mm, the resulting lattice achieves an open rate of 30.91%, which is comparable with some of the existing benchmark designs.1

In summary, the double-layered microperforated meta-shell array as acoustic ventilation barrier has been proposed and studied through both theoretical and experimental studies. Acoustic performance has been evaluated analytically using multiple scattering theory, and verified by numerical simulations. Based on theoretical exploration, experimental studies have been conducted for three different configurations of MPP meta-shell structures. For each model, two different perforation rates of the meta-shell and different cell numbers are considered. Experimental results show that insertion of inner shell helps to improve the absorption, and the enhancement effect may depend on the choice of perforation rates of micro cores. In addition, adding an extra layer of sponge to the MPP meta-shell can significantly improve the lowfrequency absorption as a result of the inter-cell coupling interaction. The remarkable acoustic performance together with a high ventilation rate make the proposed design a good candidate for room acoustics application where proper airflow is required.

This work was supported by Steelcase Inc. and the NSF CMMI under Award No. 1930873.

AUTHOR DECLARATIONS Conflict of Interest

The authors have no conflicts to disclose.

Author Contributions

Jiaji Chen: Formal analysis (equal); Software (equal); Writing – original draft (equal); Writing – review & editing (equal). Yonghui Zhang: Validation (equal); Writing – review & editing (equal). Yukai Yu: Investigation (equal); Software (equal); Visualization (equal). Yao Zhai: Validation (equal). Huy Quang Nguyen: Conceptualization (equal); Formal analysis (equal); Investigation (equal). Sharon Tracy: Funding acquisition (equal); Supervision (equal). Xiaoming Zhou:

Conceptualization (equal); Validation (equal); Writing – review & editing (equal). **Guoliang Huang:** Conceptualization (equal); Funding acquisition (equal); Project administration (equal); Supervision (equal); Writing – review & editing (equal).

DATA AVAILABILITY

The data that support the findings of this study are available from the corresponding authors upon reasonable request.

REFERENCES

- ¹Y. Tang, S. Ren, H. Meng, F. Xin, L. Huang, T. Chen, C. Zhang, and T. J. Lu, "Hybrid acoustic metamaterial as super absorber for broadband low-frequency sound," Sci. Rep. 7, 43340 (2017).
- ²S. Huang, X. Fang, X. Wang, B. Assouar, Q. Cheng, and Y. Li, "Acoustic perfect absorbers via Helmholtz resonators with embedded apertures," J. Acoust. Soc. Am. 145, 254–262 (2019).
- ³Y. Chen, R. Zhu, H. Nguyen, and G. Huang, "Membrane-type acoustic metamaterials: Theory, design, and application," in *Theory and Design of Acoustic Metamaterials*, edited by P. Pai and G. Huang (SPIE Press, 2015), Chap. 3, pp. 53–56.
- ⁴H. Nguyen, Q. Wu, X. Xu, H. Chen, S. Tracy, and G. Huang, "Broadband acoustic silencer with ventilation based on slit-type Helmholtz resonators," Appl. Phys. Lett. 117, 134103 (2020).
- ⁵X. Wu, K. Y. Au-Yeung, X. Li, R. C. Roberts, J. Tian, C. Hu, Y. Huang, S. Wang, Z. Yang, and W. Wen, "High-efficiency ventilated metamaterial absorber at low frequency," Appl. Phys. Lett. 112, 103505 (2018).
 ⁶S. Kumar, T. B. Xiang, and H. P. Lee, "Ventilated acoustic metamaterial win-
- 6S. Kumar, T. B. Xiang, and H. P. Lee, "Ventilated acoustic metamaterial window panels for simultaneous noise shielding and air circulation," Appl. Acoust. 159, 107088 (2020).
- ⁷X. Wu, C. Fu, X. Li, Y. Meng, Y. Gao, J. Tian, L. Wang, Y. Huang, Z. Yang, and W. Wen, "Low-frequency tunable acoustic absorber based on split tube resonators," Appl. Phys. Lett. 109, 043501 (2016).
- ⁸G. Ma, M. Yang, Z. Yang, and P. Sheng, "Low-frequency narrow-band acoustic filter with large orifice," Appl. Phys. Lett. **103**, 011903 (2013).
- ⁹J.-S. Chen, Y.-B. Chen, H.-J. Tsai, K.-Y. Chen, and L.-C. Chou, "Membranering acoustic metamaterials with an orifice," Mater. Res. Express 6, 095802 (2019).
- 10 H. Nguyen, Q. Wu, H. Chen, J. Chen, Y. Yu, S. Tracy, and G. Huang, "A Fano-based acoustic metamaterial for ultra-broadband sound barriers," Proc. R. Soc. A 477, 20210024 (2021).
- ¹¹H.-l. Zhang, Y.-f. Zhu, B. Liang, J. Yang, J. Yang, and J.-C. Cheng, "Omnidirectional ventilated acoustic barrier," Appl. Phys. Lett. 111, 203502 (2017).
- ¹²R. Ghaffarivardavagh, J. Nikolajczyk, S. Anderson, and X. Zhang, "Ultra-open acoustic metamaterial silencer based on Fano-like interference," Phys. Rev. B 99, 024302 (2019).
- ¹³L.-j. Li, B. Zheng, L.-m. Zhong, J. Yang, B. Liang, and J.-c. Cheng, "Broadband compact acoustic absorber with high-efficiency ventilation performance," Appl. Phys. Lett. 113, 103501 (2018).
- ¹⁴J. W. Jung, J. E. Kim, and J. W. Lee, "Acoustic metamaterial panel for both fluid passage and broadband soundproofing in the audible frequency range," Appl. Phys. Lett. 112, 041903 (2018).
- ¹⁵M. Thota and K. Wang, "Reconfigurable origami sonic barriers with tunable bandgaps for traffic noise mitigation," J. Appl. Phys. 122, 154901 (2017).
- ¹⁶V. M. García-Chocano, S. Cabrera, and J. Sánchez-Dehesa, "Broadband sound absorption by lattices of microperforated cylindrical shells," Appl. Phys. Lett. 101, 184101 (2012).
- ¹⁷D.-Y. Maa, "Potential of microperforated panel absorber," J. Acoust. Soc. Am. 104, 2861–2866 (1998).
- ¹⁸F. A. Amirkulova, "Acoustic and elastic multiple scattering and radiation from cylindrical structures," Ph.D. thesis (Rutgers, The State University of New Jersey, New Brunswick, 2014).
- ¹⁹Z.-x. Xu, H. Gao, Y.-j. Ding, J. Yang, B. Liang, and J.-c. Cheng, "Topology-optimized omnidirectional broadband acoustic ventilation barrier," Phys. Rev. Appl. 14, 054016 (2020).